JACS
JOURNAL OF THE AMERICAN CHEMICAL SOCIETY

ARTICLE

pubs.acs.org/JACS

Electrochemical Water Oxidation with Cobalt-Based Electrocatalysts from pH 0−14: The Thermodynamic Basis for Catalyst Structure, Stability, and Activity

James B. Gerken,[†] J. Gregory McAlpin,[‡] Jamie Y. C. Chen,[†] Matthew L. Rigsby,[†] William H. Casey,*[,‡] R. David Britt,*[,‡] and Shannon S. Stahl*[,†]

[†]Department of Chemistry, University of Wisconsin−Madison, 1101 University Avenue, Madison, Wisconsin 53706-1322, United States

[‡]Department of Chemistry, University of California, 1 Shields Avenue, Davis, California 95616-0935, United States

Supporting Information

ABSTRACT: Building upon recent study of cobalt-oxide electrocatalysts in fluoride-buffered electrolyte at pH 3.4, we have undertaken a mechanistic investigation of cobalt-catalyzed water oxidation in aqueous buffering electrolytes from pH 0−14. This work includes electrokinetic studies, cyclic voltammetric analysis, and electron paramagnetic resonance (EPR) spectroscopic studies. The results illuminate a set of interrelated mechanisms for electrochemical water oxidation in alkaline, neutral, and acidic media with electrodeposited Co-oxide catalyst films (CoO_x[cf]s) as well as for a homogeneous Co-catalyzed electrochemical water oxidation reaction. Analysis of the pH dependence of quasi-reversible features in cyclic voltammograms of the CoO_x[cf]s provides the basis for a Pourbaix diagram that closely resembles a Pourbaix diagram derived from thermodynamic free energies of formation for a family of Co-based layered materials. Below pH 3, a shift from heterogeneous catalysis producing O_2 to homogeneous catalysis yielding H_2O_2 is observed. Collectively, the results reported here provide a foundation for understanding the structure, stability, and catalytic activity of aqueous cobalt electrocatalysts for water oxidation.

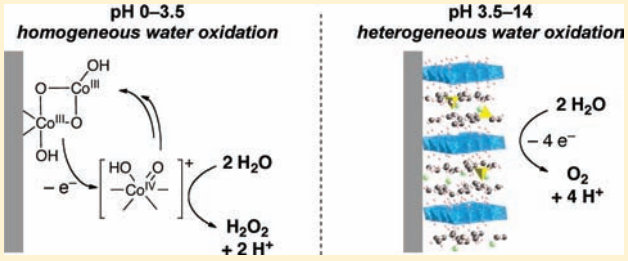

INTRODUCTION

The appeal of (photo)electrochemical water splitting (Scheme 1) as a means of storing solar energy[1] has motivated studies of electrocatalytic water oxidation for more than a half century.[2] Investigations of molecular[3] and solid-state[4] electrocatalysts capable of mediating water oxidation have targeted the development of catalysts that operate at lower overpotential and the acquisition of mechanistic insights into this critical transformation.

Our own efforts in this area are focused on the development of electrocatalysts derived from earth abundant materials, as alternatives to noble metal catalysts, such as RuO_2 and IrO_2, which are employed in electrolyzers that operate under acidic conditions (e.g., proton-exchange membrane electrolyzers).[5] Inspired by reports that $Co^{III}F_3$ and fluorocobaltate(III) salts oxidize water to O_2 with the formation of HF,[6−8] we decided to investigate the electrochemical oxidation of cobalt(II) in aqueous fluoride electrolyte. HF is a weak acid (pK_a = 3.17), and we speculated that fluoride could act as an effective proton acceptor and as an oxidatively robust ligand that could moderate the high $Co_{aq}^{II/III}$ potential (1.86 V vs normal hydrogen electrode, NHE)[9] toward the thermodynamic potential for O_2 production, thereby enabling efficient catalysis at reduced overpotential (Scheme 2). Our recently reported preliminary results[10] did not support this hypothesis. Instead of catalysis by soluble fluorocobaltate species, electrolysis of Co_{aq}^{II} in HF/F^- electrolyte results in formation of catalytically active heterogeneous cobalt-oxide catalyst films (CoO_x[cf]s). These observations closely resemble the recent results of Nocera and co-workers, who have investigated CoO_x[cf]s formed upon electrolysis of Co_{aq}^{II} in the presence of inorganic phosphate, borate, and other buffering electrolytes.[11]

Cobalt oxide materials have been studied extensively as electrocatalysts for water oxidation, most thoroughly under alkaline conditions. A table summarizing previous electrochemical studies of cobalt-catalyzed water oxidation is provided in the Supporting Information (Table S1).[4b,c,12] Examples include various structural classes of cobalt oxides and MCo_2O_4 or CoM_2O_4 spinel and $MCoO_3$ perovskite-type oxides (M = many alkaline, transition-metal, and rare-earth cations).[13] Cobalt, nickel, and mixed-metal oxide anodes are currently employed in commercial alkaline electrolyzers.[2e] In addition to the diversity of catalyst compositions, different morphologies ranging from amorphous oxides, crystalline nanoparticles, and bulk crystals have been studied.[4a−e,14] In situ formation of a CoO_x[cf] on an electrode under buffered conditions was first reported over a century ago;[15] however, its significance was not realized at the time, and systematic investigation of such films in water electrolysis applications was not pursued until the late 1960s.[14,16] The recent

Received: June 17, 2011
Published: August 01, 2011

Scheme 1. Oxidative (a) and Reductive (b) Half-Reactions for Water Splitting (c)

a) $2\,H_2O \longrightarrow O_2 + 4\,H^+ + 4\,e^-$ $E = 1.23\ V_{NHE} - 59\ mV/pH$

b) $4\,H^+ + 4e^- \longrightarrow 2\,H_2$ $E = 0\ V_{NHE} - 59\ mV/pH$

c) $2\,H_2O \longrightarrow O_2 + 2\,H_2$

Scheme 2. Initial Strategy To Achieve Catalytic Water Oxidation via Electrochemical Regeneration of $Co^{III}F_3$

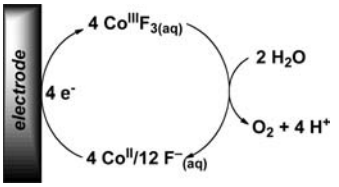

work of Nocera and co-workers[11] has drawn significant attention to CoO_x[cf]s, including opportunities to use these electrocatalysts at neutral and mildly basic pH through the appropriate selection of a buffering electrolyte. This work has also provided fundamental insights into the catalyst structure and the mechanism of water oxidation, and the utility of these CoO_x[cf]s is amplified by their recent integration with photoactive materials, such as zinc, tungsten, and iron oxides, to facilitate light-driven water oxidation.[17]

In contrast to the studies noted above, cobalt electrocatalysts for water oxidation under acidic conditions have received little attention.[18] The aqueous chemistry of cobalt solutions is complex between pH 0−5, where hydrolysis and anation of Co_{aq}^{III} is significant.[19,20] Chemical oxidants have been employed in combination with dissolved aquocobalt ions to achieve water oxidation,[21] giving hydrogen peroxide as the initial product. In the presence of Co^{III}, hydrogen peroxide undergoes disproportionation to O_2 and water; however, the kinetics and electrochemical potential for this process differ substantially from oxygen evolution mediated by CoO_x[cf]s.[22]

Fluoride is an important buffering electrolyte because it enables CoO_x[cf]-mediated electrocatalytic water oxidation to proceed under mildly acidic conditions (pH 3−4.5), a feature that has implications for integrating electrocatalytic water oxidation into artificial photosynthetic cells.[23] To provide a foundation for future applications of this type, we have undertaken a systematic mechanistic study of electrochemical water oxidation mediated by Co catalysts across a broad pH range (pH 0−14). Electrokinetic studies provide evidence for two interrelated mechanisms of water oxidation that operate under acidic (pH < ~3.5) or mildly-acidic to basic conditions (pH > ~3.5). Cyclic voltammetric and electron paramagnetic resonance (EPR) spectroscopic studies of the cobalt electrocatalysts under different conditions provide insights into the identity of cobalt species present in the CoO_x[cf]s at different pH and electrochemical potentials, including cobalt oxidation states associated with individual intermediates in the catalytic mechanisms. When these empirical pH/electrochemical potential data are plotted in the form of a Pourbaix diagram, they show a high degree of correlation with independent data derived from thermodynamic free energies of formation for different aqueous and heterogeneous cobalt species. This correlation provides a basis for the structural assignment of the active Co species involved in water oxidation and establishes a thermodynamic basis for the structure, stability, and activity of such catalysts.

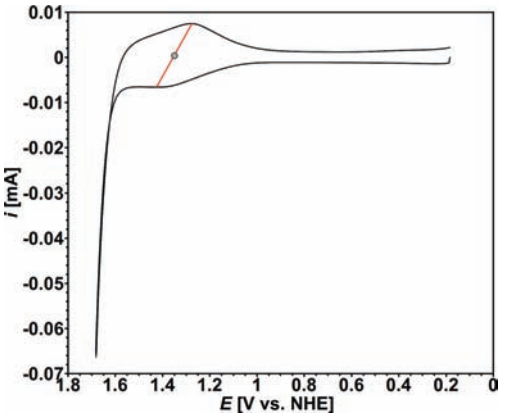

Figure 1. CV obtained with an FTO anode in 0.1 M of F^- buffer at pH 3.4 containing 0.05 mM Co^{2+} (100 mV/s). The diagonal line (red) connects the anodic (1.41 V) and cathodic (1.28 V) peaks of the quasi-reversible feature prior to the catalytic wave; a dot (gray) indicates the midpoint potential at 1.34 V.

RESULTS

Cobalt-Catalyzed Water Oxidation in Fluoride-Buffered Electrolyte. In our previous report,[10] we described cyclic voltammetry (CV) studies probing electrocatalytic water oxidation in aqueous solutions of $CoSO_4$ containing 0.1 or 1.0 M potassium fluoride as a buffering electrolyte (pH 3.4).[24] At moderate scan rates (100 mV/s), voltammograms reveal a broad feature in the anodic scan at 1.41 V, followed by a sharp onset of catalytic current at approximately 1.5 V (Figure 1). A broad feature is evident at 1.28 V in the cathodic scan that appears to combine with the 1.41 V anodic feature to form a quasi-reversible redox couple, with midpoint potential (E_{mp}) ~ 1.33 V. Sustained electrolysis at 1.48 V results in deposition of a heterogeneous film on the fluorine-doped tin-oxide (FTO) electrode, and X-ray photoelectron spectroscopy revealed that the deposit consists of a cobalt-oxygen-containing material with a small amount of fluorine: $CoO_{6.3\pm0.4}F_{0.29\pm0.04}$ for a sample deposited from 0.1 M of F^- buffer and $CoO_{6.7\pm0.3}F_{0.37\pm0.14}$ for a sample deposited from 1.0 M of F^- buffer. Analogous to observations made previously by others,[11,14a,15a] the electrodeposited cobalt-oxide film exhibits catalytic activity for water oxidation in electrolyte lacking Co ions; however, the activity of the film decreases as the coating on the electrode dissolves over time. The Co-oxide film and dissolved Co ions are in equilibrium at pH 3.4, and stable steady-state catalytic current was possible in the presence of a low concentration of soluble Co^{II} in the electrolyte (e.g., 0.1−1 mM). Monitoring oxygen evolution during steady-state electrolysis and comparing with the amount of current passed revealed ≥95% Faradaic yield of O_2 (Figure 2).

The steady-state current observed with this electrocatalytic system was monitored as a function of the applied overpotential for water oxidation, enabling the construction of a Tafel plot (Figure 3). A linear Tafel plot was obtained when electrolysis was carried out in 1.0 M F^- (black diamonds), with a slope of 60 mV/decade. In contrast, a discontinuity is evident in the Tafel plot derived from electrolysis in 0.1 M of F^- (Figure 3, gray circles and squares). At higher overpotentials and current densities, the data shift from a slope of 60 to 113 mV/decade, and this transition correlates with

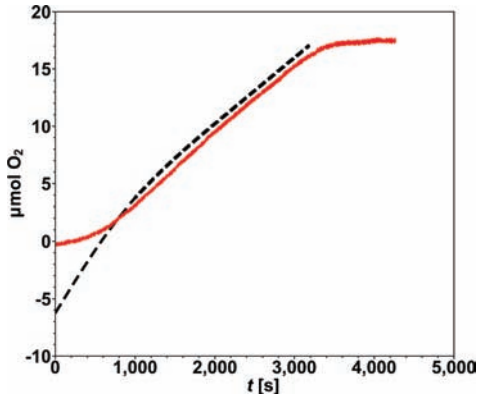

Figure 2. Theoretical (dashed black) and observed (solid red) O_2 formed as functions of time in 1.0 M and pH 3.4 fluoride buffer. Negative values of the theoretical oxygen amount reflect the charge consumed in oxidation of the Co^{2+} catalyst precursor.

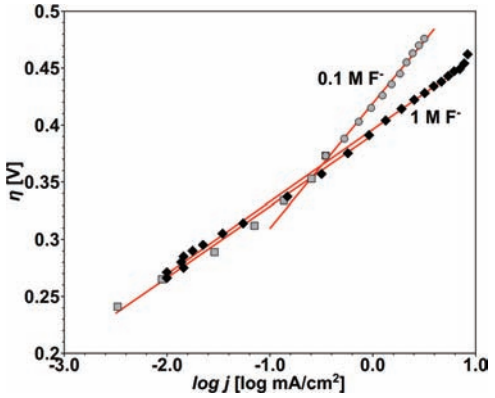

Figure 3. Steady-state Tafel data acquired with FTO anodes at pH 3.4 in 0.1 and 1 M of F^- buffers containing 1 mM of Co^{2+}. A heterogeneous deposit formed on the anode during electrolysis. A slope of 60 mV/decade was observed in 1 M of F^- (black diamonds) and at low current densities in 0.1 M of F^- (gray squares). At high current density in 0.1 M F^- (gray circles), a slope of 113 mV/decade was observed, together with dissolution of the heterogeneous catalyst film.

dissolution of the film from the electrode surface. In order to gain a thorough understanding of the mechanistic origin of this behavior, we investigated a systematic series of cobalt catalyst systems for electrochemical water oxidation across a broad pH range.

Tafel Analysis of Cobalt-Catalyzed Electrochemical Water Oxidation From pH 0−14. Preliminary studies of Co-catalyzed electrochemical water oxidation revealed different behavior under three sets of conditions: (1) at pH ≥ ∼5.5, electrodeposited Co-oxide catalyst films are stable, and sustained electrolysis is observed without including additional Co^{II} in the buffering electrolyte; (2) at ∼3 ≤ pH ≤ ∼5.5, a heterogeneous Co-oxide electrocatalyst exists in dynamic equilibrium with dissolved cobalt ions, and the CoO_x^{cf} dissolves during sustained electrolysis if insufficient cobalt ion concentration is present in solution; and (3) at pH ≤ ∼3, the CoO_x^{cf} dissolves, and no heterogeneous deposit is evident on the electrode during electrochemical water oxidation.

On the basis of these observations, systematic electrochemical studies of CoO_x^{cf}s and Co^{II}/electrolyte solutions were conducted in the following manner. For studies above pH 5.5, one of two methods was used to prepare the CoO_x^{cf}. In the first approach, based on the method of Chen and Noufi,[14a] a CoO_x^{cf} was electrodeposited from a 0.1 mM solution of Co^{II} dissolved in acetate electrolyte (pH 7.0) onto a FTO electrode. The resulting coated electrode was then used to perform Tafel studies in solutions of various buffering electrolytes. In the second method, based on the recent studies of Nocera and co-workers,[11] the CoO_x^{cf} was electrodeposited from 0.1 mM solutions of dissolved Co^{II} ions in an electrolyte of interest. Tafel data were then obtained from a fresh solution of the same electrolyte lacking dissolved cobalt ions. With each of these methods, catalyst depositions of 30−60 mC/cm^2 led to the formation of well-behaved CoO_x^{cf}s that exhibited reproducible Tafel behavior (see below). This deposition charge-density produces thin-film catalysts with minimal potential drop within the film thickness.[11f] For studies carried out below pH 5.5, dissolved cobalt ions were needed to ensure steady-state stability of the CoO_x^{cf} (3 ≤ pH ≤ 5.5) or to serve as a homogeneous electrocatalyst (pH ≤ 3), and the Tafel electrolysis experiments were performed directly in the Co^{II}/electrolyte solution (initial $[Co^{II}]$ = 1 mM). A control experiment performed at pH 1 under cobalt-free conditions confirmed the electrocatalytic activity of cobalt under acidic conditions.

The desired pH for these Tafel studies was established by employing an appropriate buffering electrolyte, and the analysis was performed with 0.1 and 1.0 M electrolyte concentrations (Figure 4). It was necessary to allow passage of sufficient charge at each potential step to ensure the system reached a steady state in order to obtain reproducible linear Tafel plots.[25] Qualitatively, phosphate and fluorophosphate buffers at pH 7 and 4.8, respectively, led to films with somewhat diminished activity, and the deposition in 1 M of phosphate at pH 7 led to a gradual decay of catalytic activity, even once quasi-steady-state current densities were achieved (see Supporting Information). The exchange current appears to follow no clear trend with buffer pH over 10 orders of magnitude in proton concentration (pH 3.5−14). The variations that are observed may be due to surface coverage or inhibition by buffers that can compete with water binding to the catalyst.[26] Slopes and exchange currents observed in this work are listed in Table S2, Supporting Information.

The Tafel data in Figure 4 provide evidence for two different mechanistic regimes. Above pH 4, the anode deposit gave a consistent Tafel slope of 50−70 mV/decade with an exchange current that was not pH or buffer dependent. At pH 2 and below, no CoO_x^{cf} deposit forms, and CoO_x^{cf}s prepared ex situ on FTO electrodes rapidly dissolve when current is passed. The Tafel data obtained under these acidic conditions result in a slope of 110−130 mV, with a pH-dependent, but buffer-independent, exchange current. These results may be compared to the Tafel plot obtained with fluoride buffer at pH 3.4, for which the 0.1 M data exhibit features consistent with both mechanistic regimes (i.e., a change in the Tafel slope from 60 to 113 mV/decade and a transition from a heterogeneous to a homogeneous Co catalyst), depending on the current density (Figure 3). As discussed further below, these observations are consistent with a change in the catalyst identity and the rate-determining step of water oxidation at a pH between 3−3.5.

Electrocatalytic water oxidation with the homogeneous Co catalyst under acidic conditions was analyzed to establish the dependence of the rate on [Co] and $[H^+]$. At pH 1, electrolysis was performed at a potential of 1830 mV vs NHE with variable amounts of initial $[Co^{II}]$ in solution. Steady-state currents exhibit a saturation dependence on the cobalt concentration (Figure 5). In light of the formation of heterogeneous Co-oxide films at a

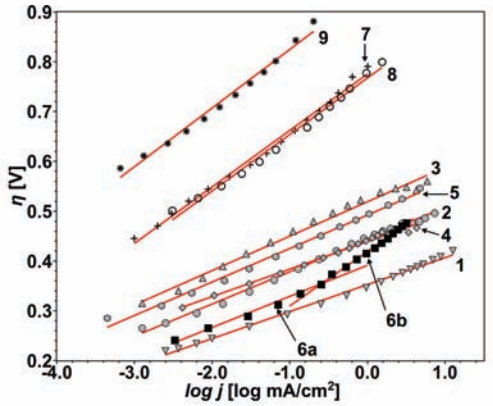

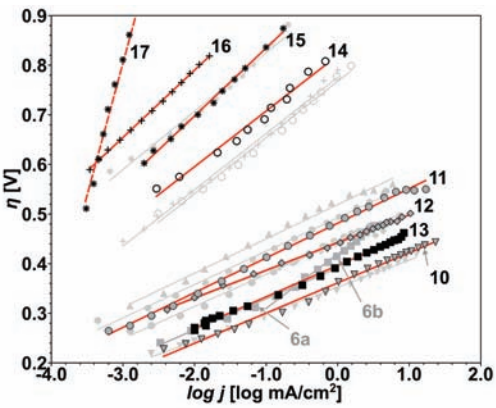

Plot #	pH	Electrolyte Composition	Catalyst Formation and/or Composition	Tafel Slope (mV/decade)
1	13	0.1 M NaOH	ex-situ Co-free sol'n	54
2	7	0.1 M phosphate	in-situ Co-free sol'n	65
3	7	0.1 M phosphate	ex-situ Co-free sol'n	69
4	6.3	0.1 M $TfNH_2$	in-situ Co-free sol'n	55
5	4.8	0.1 M $HFPO_3^-$	in-situ [Co] = 1 mM	67
6a	3.4	0.1 M fluoride	in-situ [Co] = 1 mM	60 (low η)
6b	3.4	0.1 M fluoride	no film [Co] = 1 mM	113 (high η)
7	2.1	0.1 M sulfate	no film [Co] = 1 mM	113
8	2	0.1 M phosphate	no film [Co] = 1 mM	113
9	1	0.1 M BF_4^-	no film [Co] = 1 mM	118

Plot #	pH	Electrolyte Composition	Catalyst Formation and/or Composition	Tafel Slope (mV/decade)
10	14	1 M NaOH	ex-situ Co-free sol'n	61
11	7	1 M phosphate	in-situ Co-free sol'n	70
12	6.3	1 M $TfNH_2$	in-situ Co-free sol'n	56
13	3.4	1 M fluoride	in-situ [Co] = 1 mM	60
6a	3.4	0.1 M fluoride	in-situ [Co] = 1 mM	60 (low η)
6b	3.4	0.1 M fluoride	no film [Co] = 1 mM	113 (high η)
14	2	1 M phosphate	no film [Co] = 1 mM	112
15	1	1 M BF_4^-	no film [Co] = 1 mM	137
16	0.3	1 M sulfate	no film [Co] = 1 mM	135
17	1	1 M BF_4^-	Control [Co] = 0	529

Figure 4. Tafel plots for cobalt-catalyzed electrochemical water oxidation performed in the various buffering electrolytes listed.[27] CoO_x^{cf} films formed in situ were then electrolyzed in an identical electrolyte buffer, either with or without soluble cobalt. Films formed ex-situ were prepared by Noufi's method.[14a] In 0.1 M of F^- at pH 3.4 and at current densities greater than the break in slope (plot 6b), the CoO_x^{cf} is unstable.

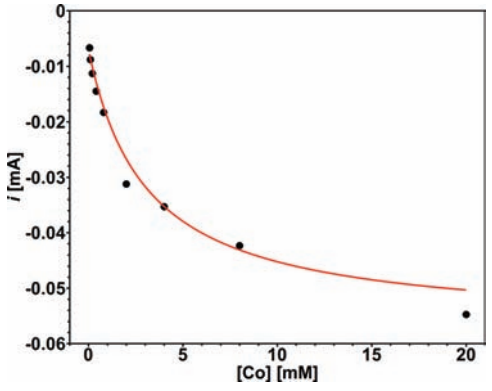

Figure 5. Plot of cobalt-catalyzed electrochemical water oxidation current as a function of cobalt concentration in pH 1 0.1 M of sulfate at 1830 mV vs NHE. Circles are experimental data; line is a fitted Langmuir isotherm (eq 1; $R^2 = 0.987$).

higher pH, we hypothesize that these results arise from a cobalt adsorption process that occurs prior to the rate-limiting step at this pH (see Discussion Section). Reflecting this interpretation, the data can be fit to a Langmuir isotherm (eq 1 and curve fit in Figure 5). Constant-current electrolysis at $-10\ \mu A/cm^2$ was performed in the presence of 1 mM of cobalt, while the pH was varied from 0.15 to 2. Steady-state potentials plotted versus pH (Figure 6) reveal a 121 mV/pH trend, consistent with a 2 H^+/e^- process.

$$i(\text{mA}) = -0.007 - 0.05\left(\frac{0.325[\text{Co}]}{1 + 0.325[\text{Co}]}\right)(\text{mM}) \qquad (1)$$

Electrolyses performed under conditions that are compatible with a stable CoO_x^{cf} result in near-quantitative Faradaic yields for O_2 evolution (e.g., see Figure 2),[28] as has been observed previously.[4,10,11] In contrast, electrolysis of 1 mM of Co in 0.1 M tetrafluoroborate electrolyte with η = 680 mV at pH 2.1 (1.79 V vs NHE) showed initial Faradaic efficiencies far from unity followed by an increase in the O_2 production rate, eventually reaching a plateau at the expected value (Figure 7). This observation is consistent with studies of Co-mediated water oxidation under acidic conditions using chemical oxidants, which support the formation of hydrogen peroxide as the water oxidation product.[21] Treatment of aliquots of the anolyte with iodide showed signs of peroxide through the formation of the brown-colored I_3^- ion.[29] The ability of cobalt to catalyze the disproportionation of H_2O_2[30] prevented quantitation of H_2O_2 yields in the acidic electrolysis solutions.

CV Studies of Cobalt-Containing Electrolytes From pH 0−14. CVs of CoO_x^{cf}s reveal the presence of quasi-reversible redox couples at potentials lower than the catalytic wave (cf. Figure 1 and

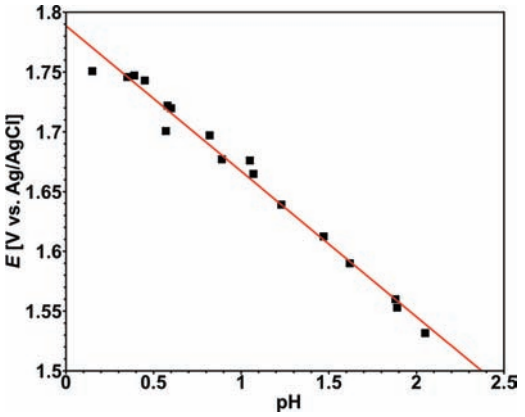

Figure 6. Plot of potential (vs Ag/AgCl) for cobalt-catalyzed electrochemical water oxidation performed at $-10\ \mu A/cm^2$ in 1.0 M of sulfate (slope of -121 mV/pH) as a function of pH.

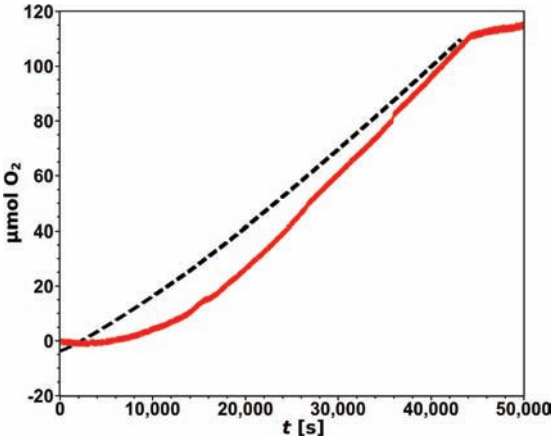

Figure 7. Theoretical (dashed black) and observed (solid red) oxygen amounts as functions of time in 0.1 M and pH 2.1 tetrafluoroborate buffer (1.79 V vs NHE). O_2 concentrations were monitored with a fluorescence-quench probe (see Supporting Information for details).

previous reports[11b,12a,14a,31]). In order to perform a systematic analysis of these features, CVs were acquired from pH 2−13 by employing a number of different buffering electrolytes, including hydroxide, vanadate, carbonate, borate, methylphosphonate, phosphate, trifluoromethanesulfonamide, fluorophosphate, fluoride, and sulfate. The number and the position of the redox couples are dependent upon the pH of the electrolysis solution (Figure 8). At and above pH 8, two distinct redox processes are evident (Figure 8a−e), which exhibit different dependencies on the pH (see below and Supporting Information). From pH 3−8, the prefeatures merge with each other, and only one redox couple is observed at potentials below the catalytic wave (Figure 8f−i). At pH ≈ 3, the anodic process disappears into the catalytic wave, leaving only a broad cathodic peak (Figure 8j and k). Below this pH, no heterogeneous deposit is observed. Even under acidic conditions, however, an increase in current relative to background is observed in electrolytes with millimolar concentrations of cobalt ions. Similar cyclic voltammograms were observed with FTO anodes coated with Co_3O_4 nanoparticles (Figure S4, Supporting Information),[4c] indicating that the redox processes preceding catalysis are independent of the initial form of the catalyst.

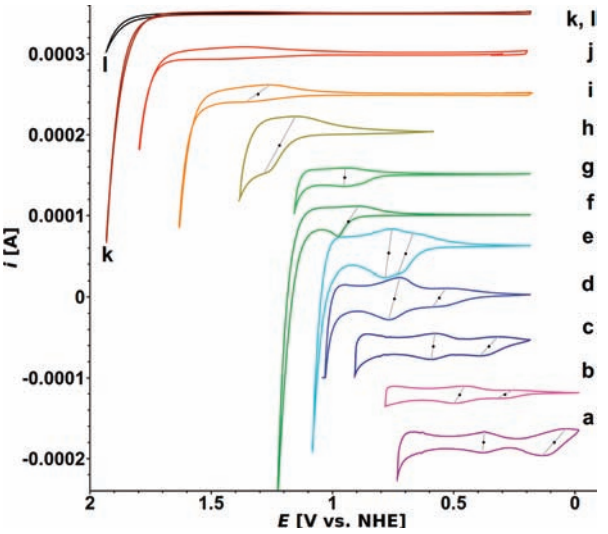

Figure 8. Representative cyclic voltammograms of CoO_x^{cf}s on FTO anodes obtained by scanning at 1 mV/s in the electrolytes buffered at the indicated pH: (a) pH 13 hydroxide, (b) pH 11.6 vanadate, (c) pH 10.3 carbonate, (d) pH 9.2 borate, (e) pH 8 methylphosphonate, (f) pH 7.0 phosphate, (g) pH 6.3 trifluoromethylsulfonamide (vertical scale reduced 10×), and (h) pH 4.8 fluorophosphate. CVs obtained from electrolyte solutions containing 0.5 mM of $CoSO_4$: (i) pH 3.4 fluoride, (j) pH 2.1 phosphate, and (k) pH 2.0 sulfate; and (l) Co-free pH 2 background. Gray lines indicate the quasi-reversible redox couples, and black dots identify the corresponding midpoint potentials. Potentials are relative to NHE, and currents are vertically offset for visibility.

Midpoint potentials for the quasi-reversible redox couples were established from the peak potentials of the corresponding anodic and cathodic features (see gray lines and black dots on the CVs in Figure 8). For cases in which overlapping features obscured peak positions, inflection points were identified from the derivative of the CV trace (Figure S5, Supporting Information). Scan-rate variation showed little effect on the midpoint potentials determined by this method (Figures S6−S8, Supporting Information). The midpoint potentials, together with the potential of the catalytic waves, were plotted as a function of pH (Figure 9), and the data show a high degree of correlation with a Pourbaix diagram derived from literature data for standard free energies of formation for soluble and insoluble cobalt aquo/hydroxide/oxide species.[32,33] This correlation enables the quasi-reversible CV features to be assigned to known pH-dependent redox processes for aqueous cobalt, in cases for which free energies of formation are available.[34] As an example, the first redox process observed in the pH ∼ 8−9.5 range can be assigned to the oxidation of soluble $Co^{II}(OH_2)_6$ to an insoluble cobalt oxyhydroxide material with concomitant loss of three protons (eq 2).[35] A full set of equilibria associated with the observed redox processes is provided in the Supporting Information. As discussed further below, this Pourbaix analysis has important implications for understanding the redox events that occur in the formation of the CoO_x^{cf} from dissolved cobalt ions and within the CoO_x^{cf} after it forms on the electrode and the identity of the active cobalt-oxide species involved in water oxidation.

$$Co_{aq}^{2+} \rightleftharpoons Co(O)OH + 3H^+ + e^-$$
$$E = 1.747V - 0.059 \log[Co_{aq}^{2+}] - 0.177pH \quad (2)$$

EPR Spectroscopic Analysis of CoO_x^{cf}s. EPR spectroscopy has been used previously to establish the presence of Co^{II} and

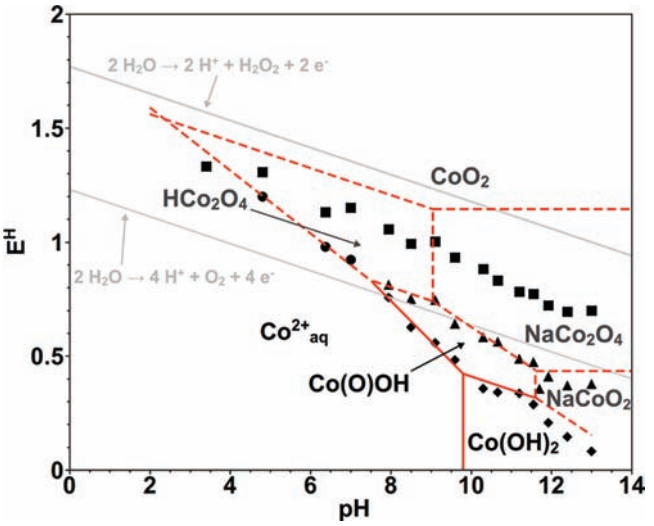

Figure 9. Pourbaix diagram showing the pH/potential characteristics of the precatalytic features evident in CVs, such as those in Figure 8, obtained from CoO_x^{cf}s in diverse buffering electrolytes. Symbols denote the following redox features: ■, potential at which the catalytic wave in the CV is equal in magnitude to the anodic prefeature; ◆, position of the midpoint potential for the first quasi-reversible wave; ▲, position of the midpoint potential for the second quasi-reversible wave; and ●, position of the midpoint potential in cases where only a single prefeature is observed. Solid red lines show the pH/potential equilibria of soluble and insoluble cobalt oxide and hydroxide species shown in black with $[Co^{2+}] = 10^{-7}$ M from data in ref 32; dashed lines indicate equilibria for species shown in gray calculated from experimental data.[33]

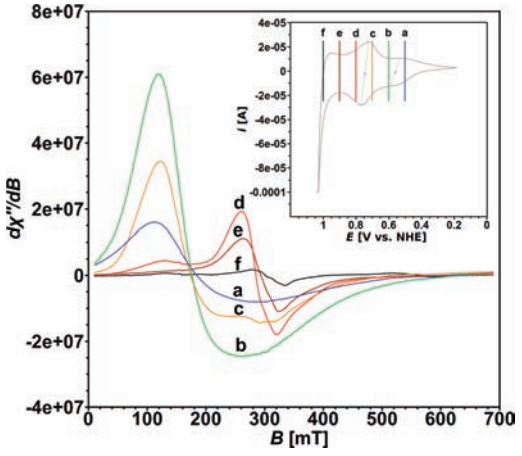

Figure 10. X-band EPR spectra acquired at 6 K on CoO_x^{cf} deposited from pH 9 borate buffer at: (a) 500, (b) 600, (c) 700, (d) 800, (e) 900, and (f) 1000 mV (microwave frequency = 9.481 GHz). Intensities are scaled to the mass of each sample with uniform acquisition parameters. Inset shows a cyclic voltamogram acquired at the same pH with the potentials of each sample indicated by vertical bars.

Co^{IV} sites in heterogeneous cobalt oxide materials,[36,37] including the recent detection of Co^{IV} in phosphate-buffered CoO_x^{cf}s.[11d] We have used similar methods to analyze CoO_x^{cf}s obtained from different electrolysis conditions in order to facilitate characterization of the redox changes within the catalyst and identify the formation of Co^{IV}-containing species at different pH and applied potential.

Table 1. X-Band g_{eff} Values of CoO_x^{cf} Samples Prepared at Various Potentials in Borate and Fluoride Buffers[a]

potential (mV vs NHE)	Co(IV) g_{eff}
pH 9 Borate Deposition	
700	2.39
800	2.36
900	2.29
1000	2.23
pH 3.4 Fluoride Deposition	
1430	2.23
1580	2.23
1580[b]	2.31
1680	2.29

[a] CoO_x^{cf} samples were prepared from borate- or fluoride-buffered electrolyses and stored at 77 K, following an ~12 min sample preparation time. See Supporting Information for details. [b] CoO_x^{cf} sample maintained at ambient temperature for an additional 10 min prior to cooling to 77 K.

Continuous-wave (CW) EPR spectra were recorded under nonsaturating, slow-passage conditions at 6 K. A series of X-band (ca. 9.5 GHz) spectra were obtained from samples formed at pH 9 in borate buffer at applied potentials ranging from 500−1000 mV vs NHE (Figure 10). At 500 and 600 mV vs NHE, the EPR spectrum is dominated by a broad derivative line shape with peak intensity at ~120 mT. This signal is characteristic of an octahedral high-spin (S = 3/2) Co^{II} species,[11d,38] which could reflect residual Co^{II}_{aq} from the deposition buffer or Co^{II} sites in a predominantly Co^{III} material.[39] The spectra lack a signal characteristic of tetrahedral Co^{II},[38a] suggesting that little or no Co_3O_4 is present in these samples.[40] The increase in the S = 3/2 Co^{II} signal from 500 to 600 mV probably arises from decreased interactions between Co^{II} sites which become more dilute in a low-spin Co^{III} matrix at higher potential.[41] Beginning at 700 mV, a feature at $g_{eff} \approx 2.3$ is observed, and as the potential is increased to 800 mV, the $g_{eff} \approx 2.3$ signal intensity increases with a concomitant decrease in the Co^{II} signal. This $g_{eff} \approx 2.3$ signal is similar to the EPR signal recently observed from CoO_x^{cf}s prepared in phosphate-buffered electrolyte, which was assigned to a Co^{IV} species.[11d] Further support for this assignment comes from the similarity of these signals to those observed in Na_xCoO_2 ($0.65 \leq x \leq 0.75$) samples.[42] In addition, Mössbauer spectroscopic evidence has been reported for Co^{IV} in Co-oxide films produced by a similar borate-buffered electrodeposition procedure.[43] As the potential is raised from 800 to 1000 mV, the signal decreases in intensity and shifts slightly to higher resonant fields (Table 1). The origin of this phenomenon is not certain, but it can be rationalized by an increased concentration of Co^{IV} in the higher-potential films, creating a magnetically nondilute environment. Spin−spin, dipolar-broadening interactions between Co^{IV} sites could explain the reduction in signal intensity and the shift in the effective g-value. A similar effect has been observed previously in related Co^{IV}-containing materials.[42] The correlation between the CV features (see inset, Figure 10) and the changes in EPR signals associated with the consumption of Co^{II} and formation of Co^{IV} observed at pH 9 (Figure 10) indicates that the two quasi-reversible CV features correspond to $Co^{II} \rightarrow Co^{III}$ and $Co^{III} \rightarrow Co^{IV}$ redox steps. The observation that Co^{IV} first appears at 700 mV, but significant catalytic turnover does not arise until ~950 mV (see inset, Figure 10), indicates that the mere

presence of Co^{IV} in the film is not sufficient to induce catalytic water oxidation.

The presence of Co^{IV} in CoO_x^{cf}s at other pH values and electrode potentials was probed via X-band EPR spectroscopy. CoO_x^{cf} samples included those obtained from fluoride (pH 3.4, 1430−1680 mV), phosphate (pH 7, 1250 mV), carbonate (pH 10.3, 1350 mV), and hydroxide (pH 13, 0.582 mV) electrolytes. An EPR signal consistent with the presence of Co^{IV} ($g_{eff} \approx 2.2-2.4$), similar to those detected in borate- and phosphate-buffered films, was evident in each of these samples (Figure 11, Table 1, and Figure S15, Supporting Information). In addition, a feature was observed at $g_{eff} = 1.99$ in the spectrum of the CoO_x^{cf} sample prepared in fluoride-buffered electrolyte at 1480 mV, a potential at which catalytic water oxidation is significant (Figure 12a). A CW Q-band (ca. 34 GHz) spectrum of this sample was also obtained, allowing better resolution of the system (Figure 12b). This spectrum exhibits a broad signal with observed g-values of 2.59, 2.17, and 1.99. A narrower signal with an observed g-value = 1.995 is also evident. These results indicate that multiple paramagnetic species are present during catalytic water oxidation, possibly arising from distinct types of Co^{IV} sites in the catalyst with different coordination environments and/or the formation of an oxygen-centered radical. Efforts to identify the sources of these reproducibly observed signals are ongoing; however, these preliminary data suggest high-frequency EPR studies should enable more-thorough electronic structural characterization of the high-oxidation-state sites formed in CoO_x^{cf}s during catalytic turnover.

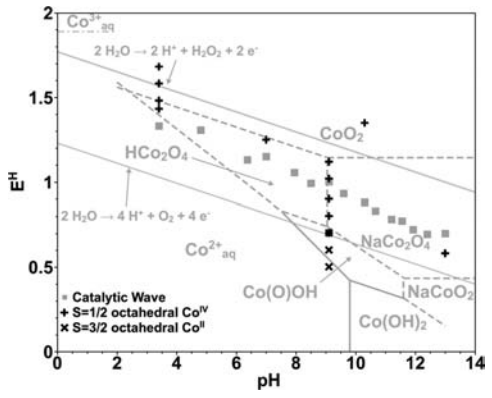

Figure 11. Identification of pH/electrode potential conditions at which CoO_x^{cf} samples were prepared and analyzed by EPR spectroscopy. The symbols, + and ×, denote the cobalt EPR signal obtained under the indicated conditions: + corresponds to an EPR signal associated with low-spin Co^{IV}, × corresponds to an EPR signal associated with octahedral S = 3/2 Co^{II}, and gray ■ indicates the potentials for the catalytic wave. At 700 mV applied potential in pH 9 borate electrolyte, both EPR signals are observed.

■ DISCUSSION

In recent years, Nocera and co-workers[11] and others[44,45] have provided key insights into the identity and the catalytic mechanism of CoO_x^{cf}s.[46] The present data expand upon the previous work in at least two significant ways: (1) the Pourbaix analysis and EPR spectroscopic studies establish a rigorous foundation for assigning the structural identity and redox states of the CoO_x^{cf}s under different conditions, including the species involved in the water oxidation reaction, and (2) the electrokinetic data provide the basis for an interrelated set of mechanisms that account for catalyst formation and water oxidation under a wide range of conditions, from pH 0−14.

The electrochemical features present in the CVs of the CoO_x^{cf}s exhibit a high degree of correlation with a Pourbaix diagram derived from thermodynamic properties of a series of cobalt-oxide layered structures. The simplest hydrous $Co(OH)_2$ structure features layers of octahedral Co^{II} coordinated by basal μ_3-OH ligands.[47] An octahedral coordination environment for Co^{II} in the CoO_x^{cf}s is supported by EPR spectroscopic data acquired from samples prepared at low potentials, as these data are inconsistent with tetrahedral Co^{II} sites, such as those present in Co_3O_4 spinel structures. The pH-dependent redox processes in the CoO_x^{cf}s (Figure 9)[48] can be readily accommodated in these "layered double-hydroxide" structures because the layers can sustain oxidation-state changes at cobalt, while retaining the same metal coordination geometries and the overall layered structure.[49] Increases in the layer charge resulting from $Co^{II} \rightarrow Co^{III} \rightarrow Co^{IV}$ oxidation and decreases in charge arising from O_2 evolution can be compensated by proton transfers involving μ_3-OH or μ_3-O bridging ligands or by rapid movement of counterions into and out of the interlayer (Figure 13). The location and identity of the interlayer ions are nonspecific, but conjugate bases of weak acids (e.g., F^-, HPO_4^{2-}) can mediate proton transfers in concert with electron-transfer reactions.[50] The spatial extent of the layered structures is constrained by previously reported X-ray diffraction data, which indicate that the CoO_x^{cf}s do not exhibit long-range order and limit the size of any crystallites to dimensions of 10−100 Å.[10,51,52] Therefore, we propose that the amorphous bulk films are composed of an ensemble of polydisperse and oligomeric, yet layered, cobaltate structures.[53]

This layered structure model, which emerges from the Pourbaix analysis, complements and elaborates upon the CoO_x^{cf}

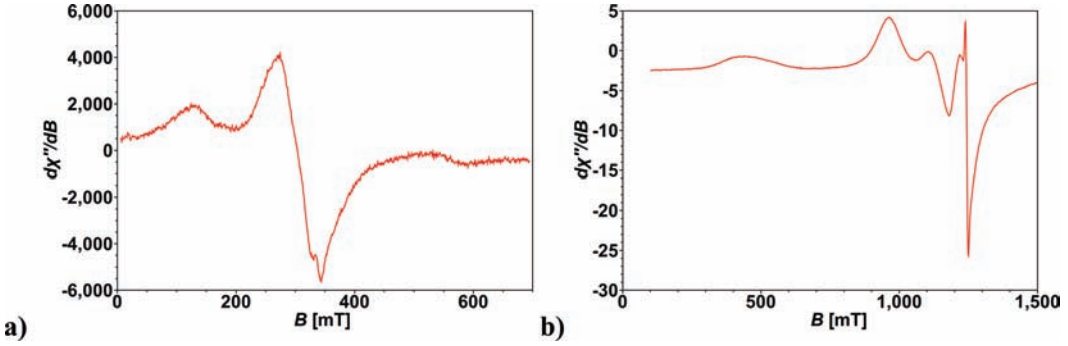

Figure 12. CW EPR spectra acquired at 6 K on CoO_x^{cf} deposited from pH 3.4 F^- buffer at 1480 mV vs NHE at: (a) X-band (microwave frequency = 9.481 GHz, T = 6 K, and microwave power = 1.0 mW) and (b) Q-band (microwave frequency = 34.766 GHz, T = 10 K, and microwave power = 0.06 mW).

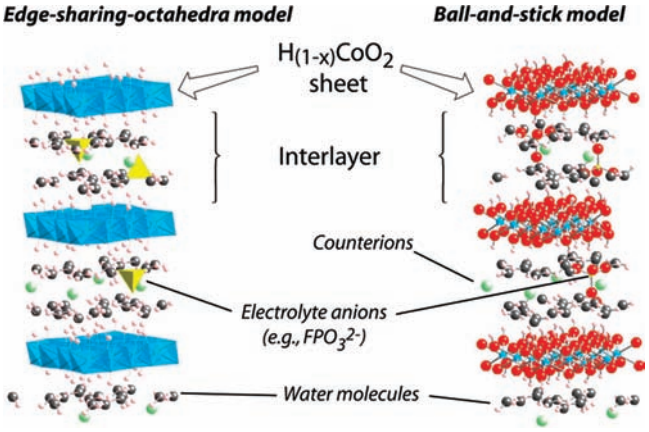

Figure 13. Depiction of cobalt-oxide layered structures that can undergo pH-dependent redox changes without large lattice variations. During catalytic water oxidation, counterion movements and proton transfers can rapidly compensate for changes in layer charge arising from changes in the cobalt oxidation states.

structures proposed on the basis of short-range structural information obtained from extended X-ray absorption fine structure (EXAFS) data. Dau et al. proposed that the catalyst is composed of mixtures of complete and incomplete cobalt-oxo cubanes,[44] whereas Nocera, Yachandra, and co-workers favored a structure composed of tiled, edge-sharing octahedra.[11e] Our data are more consistent with the latter and further suggest that the oligocobaltate lamellae are stacked, resulting in a three-dimensional layered double-hydroxide structure. The nature of the EXAFS technique limits its ability to provide information about the extent to which the oligocobaltates form layers or their polydispersity.[54] The oxidation-state assignments derived from X-ray absorption spectroscopy (XAS) data are in accord with those expected on the basis of the Pourbaix diagram shown in Figure 9. The large degree of hydration and nonstoichiometric incorporporation of electrolyte anions that we[10] and others[55] have observed via XPS analysis of CoO_x^{cf}s is consistent with a hydrous layered double-hydroxide structure.[56] This hydrated structure is supported by reports that electrochemically produced, layered α-Co(O)OH·nH_2O can exhibit a hydration number, n, that is dependent upon the electrolyte.[57]

Cobalt-based layered double-hydroxides have been studied extensively in other contexts.[49] These materials are often assigned a heterogenite stoichiometry [i.e., Co(O)OH(s)]; however, several polytypes can arise upon oxidation, differing in the placement of interlayer ions and the alignment of the stacked layers.[58] Deprotonation of layered-double-hydroxide Co(O)OH materials in the presence of an appropriate counterion produces the well-known layered cobaltates, such as $NaCoO_2$.[59] The oxidation of cobaltates is well-studied; for $M_{1-x}CoO_2$, where M = Na or Li, there has been much interest in energy storage applications.[60] Oxidized $Na_{1-x}CoO_2$ ($x > 0.6$) has been shown to react with water, although this reactivity has not been studied in the context of catalytic water oxidation.[61] Materials consisting of $H_{1-x}CoO_2$ have received less thorough attention;[58,62] however, analogous $Mn^{III/IV}$ oxide minerals are known as birnessite and buserite, which are distinguished by the presence of a layer of water molecules in buserite that form a hydrogen-bond network between the metal oxide layers present in the original brucite-like layers.[63,64] The end member, CoO_2 ($x = 1$), has been the subject of considerable investigation, including recent isolation and structural characterization in pure form.[61b,65]

The Pourbaix analysis of the CoO_x^{cf}s enables the assignment of redox states within the catalyst under different conditions and the identity of the oxide species relevant to water oxidation. These oxidation-state assignments are supported by the EPR data (Figures 10−12). The formation of Co^{IV} in the CoO_x^{cf} at potentials several hundred mV below the onset of appreciable catalytic current at pH 9 and 13 implies that the resting state of the catalyst contains Co^{IV} but must undergo further oxidation at a higher potential prior to its reaction with water. Otherwise, the catalytic wave would appear in place of the quasi-reversible feature. A similar phenomenon is evident in the nonaqueous oxidation of $LiCoO_2$, wherein oxidation of the Co^{III} sites to Co^{IV} to afford CoO_2-like species requires a higher potential than that required for initial formation of Co^{IV} sites in $LiCoO_2$.[65] Appearance of the $g = 1.995$ signal in the Q-band EPR spectrum provides some preliminary evidence that the CoO_x^{cf} progresses beyond the $Co^{III/IV}$ oxidation level (Figure 12).

Co-oxide spinels (e.g., Co_3O_4) have received considerable attention in studies of catalytic water oxidation.[4b,c,13c−13g,66] Relative to layered double-hydroxide materials, spinels would require substantial rearrangements of the metal-oxide lattice during oxidation or reduction. Moreover, the lack of a tetrahedral Co^{II} EPR signal associated with Co_3O_4 spinel[40] argues against the presence of such structures in CoO_x^{cf}s. The previously reported EXAFS and XAS data also lack evidence for spinel-type structures,[11e,44] and the stability domain of Co_3O_4 spinel lies well below the thermodynamic oxidation potential for water under all pH conditions.[67,32,34] Spinel-type cobalt-oxide materials and nanoparticles that have been used in cobalt-catalyzed water oxidation display similar kinetic properties to those observed with CoO_x^{cf}s.[4c,13f,13g] In light of the redox steps and chemical reactions required to achieve water oxidation, it is reasonable to expect that the surfaces of spinel-type materials are remodeled into layered double-hydroxide-type structures during catalytic turnover. Direct evidence for this type of structural remodeling has recently been reported by Yeo and Bell.[45]

The voltametric and spectroscopic data discussed above give information about what species are present in the CoO_x^{cf} below and at potentials that induce water oxidation. The electrokinetic data provide insights into the roles these species play in the catalytic water oxidation reaction. The Tafel data in Figure 4 exhibit the same slope from mildly acidic to strongly alkaline conditions, indicating that the same mechanism (or at least a set of electrochemically similar mechanisms) is operative across a broad pH range. The pH 3−4 range appears to mark the acidic finis terrae for heterogeneous cobalt oxide, as indicated by the shift to a higher Tafel slope at lower pH and the break in the slope in 0.1 M pH 3.4 F^- buffer. The change to higher Tafel slope coincides with a decrease in oxygen production and stripping of the anode deposit during sustained electrolysis. The pH 3−4 range is also noteworthy for containing the intersection in the Pourbaix diagram (Figure 9), where a $Co^{III/IV}$-oxide (vide supra) is predicted to become capable of disproportionating to CoO_2 and aqueous Co^{II}.

The formation of a CoO_x^{cf} from an aqueous solution of Co^{II} in a buffering electrolyte (i.e., pH > 3) arises upon applying a suitably oxidizing potential to the anode. The identities of the oxidized cobalt species reflect the conditions under which the deposit is formed, as illustrated in the Pourbaix diagram. From pH ∼8−9.5, oxidation of aqueous Co^{II} results in formation of a heterogeneous

Scheme 3. Deposition of CoO_x^{cf} and CoO_x^{cf}-Catalyzed Water Oxidation under Mildly-Acidic to Basic Conditions with Buffering Electrolytes[a]

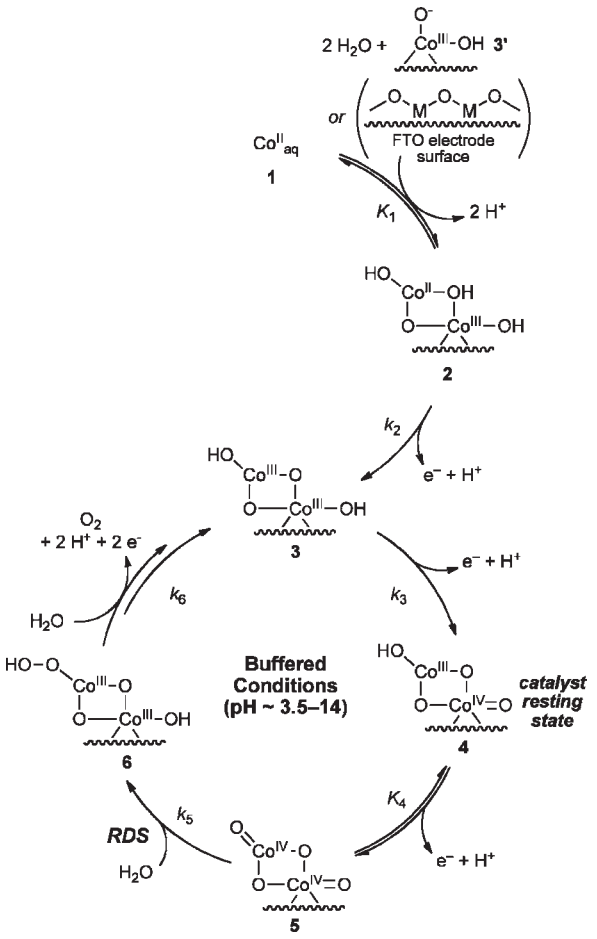

[a] Cobalt oxide intermediates shown are shorthand for adsorbed sites on the electrode surface or a layered double-hydroxide material as depicted in Figure 13. Oxo species are depicted schematically and may have significant O-centered radical character and/or a bond order other than 2. Step 6 is a composite of several rapid reactions that take place after the rate-limiting step.

Co(O)OH material, which corresponds to a 3 H^+/e^- process (Scheme 3; **1** → **2** → **3**). Subsequent 1 e^- oxidation of this material and concomitant loss of a proton produces the $Co^{III/IV}$ catalyst resting state, **4**. Under mildly acidic-to-neutral conditions (pH ~ 3−8), the Co(O)OH material is thermodynamically unstable, and oxidation of aqueous Co^{II} results in the deposition of the $Co^{III/IV}$ material **4**. This process is associated with a 7 $H^+/3$ e^- trend.[68] Under basic conditions (pH ~10−12), oxidation of heterogeneous $Co^{II}(OH)_2$ (**2**) proceeds in a stepwise process, **2** → **3** → **4** at discrete oxidation potentials. Under these conditions, **4** is deprotonated. This mechanism for formation of CoO_x^{cf}s at oxidizing potentials suggests that the 'self-healing' nature of the CoO_x^{cf}s is an emergent property of the underlying thermodynamics of the system.

Tafel plots acquired from buffered conditions from pH ~3.5−14 exhibit a slope of ~60 mV/decade. Much effort has been expended in the theoretical analysis of Tafel slopes associated with multistep electrochemical processes,[2e,f,13a,46,69] and this slope is consistent with a mechanism that has one electrochemical preequilibrium step preceding a rate-limiting chemical

Scheme 4. Oxidation of Water Catalyzed by Cobalt in Unbuffered Conditions[a]

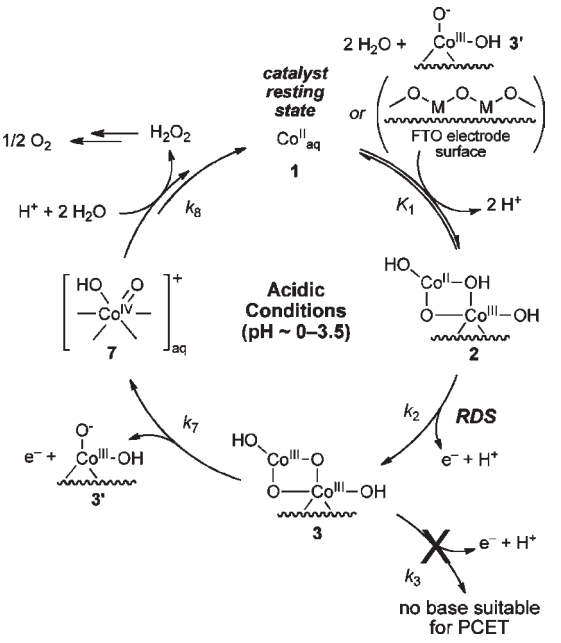

[a] Cobalt oxide intermediates shown are shorthand for adsorbed sites on the electrode surface or a layered double-hydroxide material, such as those shown in Figure 13, which is in the process of being stripped from the electrode. Oxo species are depicted schematically and may have significant O-centered radical character and/or a bond order <2.

step. Other electrochemical steps prior to the rate-limiting step (such as those related to catalyst deposition) are driven to completion at significant overpotentials and do not contribute to the observed Tafel kinetics. A mechanism similar to Scheme 3 has been elaborated recently by Nocera et al. in the context of CoO_x^{cf}-catalyzed water oxidation from pH ~7−9.[11f] The present data reveal that a similar mechanism is retained over a broad pH range. In addition, the EPR spectroscopic and cyclic voltammetric data distinguish among CoO_x^{cf} intermediates **3**, **4**, and **5** and establish that the CoO_x^{cf} exists as a $Co^{III/IV}$-oxide resting state (**4**) during catalytic turnover. According to the proposed mechanism, pre-equilibrium oxidation of **4** results in formation of a reactive CoO_2-like intermediate **5** that undergoes rate-limiting O−O bond formation. The latter step probably involves a reaction of water with **5**, rather than a reaction between lattice oxygen atoms, because previously studied $Li_{1-x}CoO_2$ and CoO_2 materials do not evolve oxygen in the absence of water.[61,65] The Pourbaix diagram indicates that the pre-equilibrium between **4** and **5** strongly favors **4** at the potentials associated with significant catalytic current.

Below pH 3, there is no visible anode deposit, and the observed Tafel slope is ~120 mV/decade. The latter result is consistent with a mechanism involving rate-limiting one-electron transfer, with no kinetically relevant electrochemical pre-equilibria. The cobalt and pH dependence of the exchange current under acidic conditions is consistent with a nonredox adsorption/deprotonation equilibrium, **1** ⇄ **2**, indicated in step 1 of Scheme 4. Specifically, the saturation cobalt dependence reflects a Langmuir isotherm (Figure 5), and the $[H^+]^{-2}$ dependence (Figure 6) matches that expected for the loss of two protons in the formation of **2**. Oxidation of the adsorbed Co^{II} species **2** to **3** corresponds to the rate-limiting one-electron process

implicated by the Tafel data. That the rate does not increase at higher electrolyte concentration indicates that the mechanism does not proceed by general-base catalysis. The coordinating ability of certain electrolyte anions, such as phosphate, can lead to inhibition of the rate, as revealed by the shift in Tafel curves between 0.1 and 1.0 M phosphate electrolyte at pH 2 (Figure 4).[26,70]

Under acidic conditions, there is no base capable of accepting a proton upon oxidation of the Co(O)OH intermediate **3** (Scheme 4, step 3), and PCET-mediated formation of the $Co^{III/IV}$-oxide **4** is prevented. Instead, the data can be rationalized by a mechanism in which oxidation of **3** takes place to afford a Co^{IV} species **7** that dissolves from the surface, promoted by the accumulation of positive charge. The oxygen evolution data implicate the formation of H_2O_2, which subsequently undergoes disproportionation (Scheme 4, step 8).[21] Co^{IV} intermediates similar to **7** have been invoked to explain homogeneous oxidation of water to H_2O_2, catalyzed by cobalt in the presence of chemical oxidants.[21a,d] The formation of H_2O_2 from such species suggests that hydrolysis of an O−O-bonded species proceeds more rapidly than the additional oxidation steps needed to form O_2. With a heterogeneous CoO_x^{cf}, an O−O-bonded intermediate, such as **6** in Scheme 3, can undergo rapid electron transfer to other Co^{IV} sites in the material or to the electrode to enable selective evolution of O_2.

Adsorbed cobalt species are ephemeral at low pH, and aqueous Co^{II} ion **1** represents the catalyst resting state. Oxidation of the Co(O)OH species **3** (Scheme 4, step 7), which leads to stripping of cobalt from the surface, takes place after the rate-limiting step and is thus fast relative to the oxidation of the transient Co^{II} species **2**. In the unique case of 0.1 M F^- electrolyte at pH ∼3.5, the increase in Tafel slope and the dissolution of the CoO_x^{cf} at higher overpotentials suggest that the rate of one-electron oxidation of **3** exceeds the ability of the buffer to promote a PCET process at the anode. As a result, the mechanism changes from O−O bond formation mediated by heterogeneous CoO_x^{cf} to homogeneous Co^{IV} as the electode potential (and current density) increases.

CONCLUSION

In this study, electrochemical water oxidation with cobalt catalysts has been investigated from pH 0−14 by employing a number of complementary methods, including cyclic voltammetry, Tafel analysis, and EPR spectroscopy. The collective data reveal that the electrodeposition of catalytically active CoO_x^{cf}s corresponds to the formation of heterogeneous, oligomeric, cobalt-based layered double-hydroxide materials. The stability and the oxidation and protonation states of these materials reflect their instrinsic thermodynamic properties reflected in a Pourbaix diagram. The local structures of these materials are dynamic during catalytic turnover, owing to changes in the oxidation states of the cobalt atoms and the flux of protons associated with the water oxidation process. The results presented here indicate that the primary role of the buffering electrolyte is to establish the pH of the electrolysis medium. The catalytic mechanism and the reaction product are dependent on pH and dissolved cobalt concentration. At acidic pH, homogeneous catalysis leads to hydrogen peroxide production. Above pH ∼3.5, heterogeneous CoO_x^{cf}s serve as the active electrocatalyst and lead to exclusive four-electron oxidation of water to O_2. Under both conditions, O−O bond formation is proposed to arise from the reaction of water with oxo Co^{IV}, a soluble mononuclear oxo Co^{IV} species under acidic conditions, and a CoO_2-like species in the CoO_x^{cf}-catalyzed reaction.

ASSOCIATED CONTENT

Supporting Information. Full experimental details, tabulated data, additional spectra, and electrochemical kinetics explanations. This information is available free of charge via the Internet at http://pubs.acs.org.

AUTHOR INFORMATION

Corresponding Authors
whcasey@ucdavis.edu, rdbritt@ucdavis.edu, stahl@chem.wisc.edu

ACKNOWLEDGMENT

The authors thank Yogesh Surendranath and Prof. Daniel Nocera (MIT), Dr. Charlie Fry (UW-Madison), Dr. Troy Stich (UC-Davis), and Prof. Nathan Lewis (Caltech) for helpful discussions and Dr. Hiromi Konishi (UW-Madison) for assistance with powder XRD data collection. This research was supported by the NSF under CCI Powering the Planet grant CHE-0802907 (S.S.S.) and NSF grant CHE-0939178 (R.D.B.), by the US Department of Energy Office of Basic Energy Science under grant DE-FG03-02ER15693 (W.H.C.), and by NMR facility funding under NIH grant 1S10RR004981-01 and NSF grants CHE-8813550 and CHE-9629688.

REFERENCES

(1) (a) Dempsey, J. L.; Esswein, A. J.; Manke, D. R.; Rosenthal, J.; Soper, J. D.; Nocera, D. G. *Inorg. Chem.* **2005**, *44*, 6879–6892. (b) Youngblood, W. J.; Lee, S.-H. A.; Maeda, K.; Mallouk, T. E. *Acc. Chem. Res.* **2009**, *42*, 1966–1973.

(2) Recent leading references and reviews include:(a) Rüttinger, W.; Dismukes, G. C. *Chem. Rev.* **1997**, *97*, 1–24. (b) Yagi, M.; Kaneko, M. *Chem. Rev.* **2001**, *101*, 21–35. (c) Meyer, T. J.; Huynh, M. H. V. *Inorg. Chem.* **2003**, *42*, 8140–8160. (d) Sala, X.; Romero, I.; Rodríguez, M.; Escriche, L.; Llobet, A. *Angew. Chem., Int. Ed.* **2009**, *48*, 2842–2852. (e) Tilak, B. V.; Lu, P. W. T.; Colman, J. E.; Srinivasan, S. In *Comprehensive Treatise of Electrochemistry*; Bockris, J. O'M., Conway, B. E., Yeager, E., White, R. E., Ed.; Plenum: New York, 1981; Vol. 2, pp 1−97. (f) Matsumoto, Y.; Sato, E. *Mater. Chem. Phys.* **1986**, *14*, 397–426.

(3) Some recent examples include: (a) Concepcion, J. J.; Jurss, J. W.; Brennaman, M. K.; Hoertz, P. G.; Patrocinio, A. O. T.; Iha, N. Y. M.; Templeton, J. L.; Meyer, T. J. *Acc. Chem. Res.* **2009**, *42*, 1954–1965. (b) Sala, X.; Ertem, M. Z.; Vigara, L.; Todorova, T. K.; Chen, W.; Rocha, R. C.; Aquilante, F.; Cramer, C. J.; Gagliardi, L.; Llobet, A. *Angew. Chem., Int. Ed.* **2010**, *49*, 7745–7747. (c) Nakagawa, T.; Bjorge, N. S.; Murray, R. W. *J. Am. Chem. Soc.* **2009**, *131*, 15578–15579. (d) Wasylenko, D. J.; Borau-Garcia, J.; Ganesamoorthy, C.; Berlinguette, C. P. *Chem. Commun.* **2011**, *47*, 4249–4251. (e) Blakemore, D.; Schley, N. D.; Balcells, D.; Hull, J. F.; Olack, G. W.; Incarvito, C. D.; Eisenstein, O.; Brudvig, G. W.; Crabtree, R. H. *J. Am. Chem. Soc.* **2010**, *132*, 16017–16029. (f) Yin, Q.; Tan, J. M.; Besson, C.; Geletii, Y. V.; Musaev, D. G.; Kuznetsov, A. E.; Luo, Z.; Hardcastle, K. I.; Hill, C. L. *Science* **2010**, *328*, 342–345. (g) Geletii, Y. V.; Besson, C.; Hou, Y.; Yin, Q.; Musaev, D. G.; Quiñonero, D.; Cao, R.; Hardcastle, K. I.; Proust, A.; Kögerler, P.; Hill, C. L. *J. Am. Chem. Soc.* **2009**, *131*, 17360–17370. (h) Ellis, W. C.; McDaniel, N. D.; Bernhard, S.; Collins, T. J. *J. Am. Chem. Soc.* **2010**, *132*, 10990–10991. (i) Süss-Fink, G. *Angew. Chem.* **2008**, *120*, 5972–5974. (j) Dogutan, D. K.; McGuire, R., Jr.; Nocera, D. G. *J. Am. Chem. Soc.* **2011**, *133*, 9178–9180.

(4) Some recent examples include: (a) Jiao, F.; Frei, H. *Chem. Commun.* **2010**, *46*, 2920–2922. (b) Jiao, F.; Frei, H. *Angew. Chem.,*

Int. Ed. **2009**, *48*, 1841–1844. (c) Esswein, A. J.; McMurdo, M. J.; Ross, P. N.; Bell, A. T.; Tilley, T. D. *J. Phys. Chem. C* **2009**, *113*, 15068–15072. (d) Dincă, M.; Surendranath, Y.; Nocera, D. G. *Proc. Natl. Acad. Sci. U.S.A.* **2010**, *107*, 10337–10341. (e) Merrill, M. D.; Dougherty, R. C. *J. Phys. Chem. C* **2008**, *112*, 3655–3666. (f) Woodhouse, M.; Parkinson, B. A. *Chem. Mater.* **2008**, *20*, 2495–2502. (g) Dokoutchaev, A. G.; Abdelrazzaq, F.; Thompson, M. E.; Willson, J.; Chang, C.; Bocarsly, A. *Chem. Mater.* **2002**, *14*, 3343–3348. (h) Chen, G.; Delafuente, D. A.; Sarangapani, S.; Mallouk, T. E. *Catal. Today* **2001**, *67*, 341–355.

(5) Early efforts in our laboratory targeting the development of molecular Ni and Co catalysts bearing various organic nitrogen- and oxygen-donor ligands failed due to the oxidative instability of the ligand under the strongly oxidizing conditions of the aqueous electrolysis experiments. There have been recent reports of homogeneous electrocatalysis by cobalt complexes bearing organic ligands. See the work of Berlinguette and Nocera in refs 3d and 3j.

(6) (a) Priest, H. F. *Inorg. Syn.* **1950**, *3*, 171–183. (b) Ustinov, V. I.; Sukhoverkhov, V. F.; Podzolko, L. G. *Zh. Fiz. Khim.* **1978**, *52*, 610–614. (c) Klemm, W.; Brandt, W.; Hoppe, R. *Z. Anorg. Allg. Chem.* **1961**, *308*, 179–189.

(7) There is sparse mention of the anodic electrochemistry of cobalt in aqueous fluoride prior to our work: see ref 15b and Kappanna, A. N.; Talaty, E. R. *Curr. Sci.* **1958**, *27*, 18.

(8) In concentrated HF, Co salts have been electrooxidized to hexafluorocobaltate(III) complexes: (a) Cox, B.; Sharpe, A. G. *J. Chem. Soc.* **1954**, 1798–1803. (b) Meyers, M. D.; Cotton, F. A. *J. Am. Chem. Soc.* **1960**, *82*, 5027–5030.

(9) Warnqvist, B. *Inorg. Chem.* **1970**, *9*, 682–684.

(10) Gerken, J. B.; Landis, E. C.; Hamers, R. J.; Stahl, S. S. *ChemSusChem* **2010**, *3*, 1176–1179.

(11) (a) Kanan, M. W.; Nocera, D. G. *Science* **2008**, *321*, 1072–1075. (b) Surendranath, Y.; Dincă, M.; Nocera, D. G. *J. Am. Chem. Soc.* **2009**, *131*, 2615–2620. (c) Lutterman, D. A.; Surendranath, Y.; Nocera, D. G. *J. Am. Chem. Soc.* **2009**, *131*, 3838–3839. (d) McAlpin, J. G.; Surendranath, Y.; Dincă, M.; Stich, T. A.; Stoian, S. A.; Casey, W. H.; Nocera, D. G.; Britt, R. D. *J. Am. Chem. Soc.* **2010**, *132*, 6882–6883. (e) Kanan, M. W.; Yano, J.; Surendranath, Y.; Dincă, M.; Yachandra, V. K.; Nocera, D. G. *J. Am. Chem. Soc.* **2010**, *132*, 13692–13701. (f) Surendranath, Y.; Kanan, M. W.; Nocera, D. G. *J. Am. Chem. Soc.* **2010**, *132*, 16501–16509.

(12) Selected references include: (a) El Wakkad, S. E. S.; Hickling, A. *Trans. Faraday Soc.* **1950**, *46*, 820–824. (b) Wabner, D.; Grambow, C. *J. Electroanal. Chem.* **1985**, *195*, 95–108. (c) Potvin, E.; Brossard, L. *Mater. Chem. Phys.* **1992**, *31*, 311–318. (d) Gorlin, Y.; Jaramillo, T. F. *J. Am. Chem. Soc.* **2010**, *132*, 13612–13614. (e) Fujimura, K.; Matsui, T.; Izumiya, K.; Kumagai, N.; Akiyama, E.; Habazaki, H.; Kawashima, A.; Asami, K.; Hasimoto, K. *Mater. Sci. Eng., A* **1999**, *267*, 254–259. (f) El-Deab, M. S.; Awad, M. I.; Mohammad, A. M.; Ohsaka, T. *Electrochem. Commun.* **2007**, *9*, 2082–2087.

(13) (a) Bockris, J. O'M.; Otagawa, T. *J. Phys. Chem.* **1983**, *87*, 2960–2971. (b) Bockris, J. O'M.; Otagawa, T. *J. Electrochem. Soc.* **1984**, *131*, 290–302. (c) Godinho, M. I.; Catarino, M. A.; da Silva Pereira, M. I.; Mendonça, M. H.; Costa, F. M. *Electrochim. Acta* **2002**, *47*, 4307–4314. (d) Singh, R. N.; Singh, J. P.; Cong, H. N.; Chartier, P. *Int. J. Hydrogen Energy* **2006**, *31*, 1372–1378. (e) Singh, R. N.; Singh, N. K.; Singh, J. P. *Electrochim. Acta* **2002**, *47*, 3873–3879. (f) Švegl, F.; Orel, B.; Grabec-Švegl, I.; Kaučič, V. *Electrochim. Acta* **2000**, *45*, 4359–4371. (g) Singh, R. N.; Koenig, J.-F.; Poillerat, G.; Chartier, P. *J. Electrochem. Soc.* **1990**, *137*, 1408–1413.

(14) (a) Chen, Y.-W. D.; Noufi, R. N. *J. Electrochem. Soc.* **1984**, *131*, 1447–1451. (b) Shafirovich, V. Ya.; Strelets, V. V. *Nouv. J. Chim.* **1978**, *2*, 199–201. (c) Burke, L. D.; Lyons, M. E.; Murphy, O. J. *J. Electroanal. Chem.* **1982**, *132*, 247–261.

(15) (a) Coehn, A.; Gläser, M. *Z. Anorg. Chem.* **1902**, *33*, 9–24. (b) Skirrow, F. W. *Z. Anorg. Chem.* **1902**, *33*, 25–30.

(16) Suzuki, O.; Takahashi, M.; Fukunaga, T.; Kuboyama, J. US Patent 3,399,966, 1968.

(17) (a) Steinmiller, E. M. P.; Choi, K.-S. *Proc. Natl. Acad. Sci. U.S.A.* **2009**, *106*, 20633–20636. (b) Seabold, J. A.; Choi, K.-S. *Chem. Mater.* **2011**, *23*, 1105–1112. (c) Zhong, D. K.; Cornuz, M.; Sivula, K.; Grätzel, M.; Gamelin, D. R. *Energy Environ. Sci.* **2011**, *4*, 1759–1764. (d) Kay, A.; Cesar, I.; Grätzel, M. *J. Am. Chem. Soc.* **2006**, *128*, 15714–15721.

(18) Much of this work has been done in the context of cobalt's effect on the anodic overpotential during electrolytic metal refining in strongly acidic solutions (pH ≤ 1): (a) Koch, D. F. A. *Aust. J. Chem.* **1959**, *12*, 127–137. (b) Åkre, T. Electrowinning of Cobalt from Chloride Solutions: Anodic Deposition of Cobalt Oxide on DSA. *Dr.-Ing Dissertation*; Norwegian University of Science and Technology: Trondheim, Norway, 2008 and references therein.

(19) (a) Davies, G. *Inorg. Chim. Acta* **1989**, *160*, 83–86. (b) Davies, G.; Warnqvist, B. *Coord. Chem. Rev.* **1970**, *5*, 349–378. (c) Davies, G.; Warnqvist, B. *J. Chem. Soc., Dalton Trans.* **1973**, 900–902.

(20) (a) Ferrer, M.; Llorca, J.; Martinez, M. *J. Chem. Soc., Dalton Trans.* **1992**, 229–231. (b) Wangila, G. W.; Jordan, R. B. *Inorg. Chim. Acta* **2005**, *358*, 3753–3760.

(21) (a) Brunschwig, B. S.; Chou, M. H.; Creutz, C.; Ghosh, P.; Sutin, N. *J. Am. Chem. Soc.* **1983**, *105*, 4832–4833. (b) Elizarova, G. L.; Matvienko, L. G.; Lozhkina, N. V.; Parmon, V. N.; Zamaraev, K. I. *React. Kinet. Catal. Lett.* **1981**, *16*, 191–194. (c) Elizarova, G. L.; Matvienko, L. G.; Lozhkina, N. V.; Parmon, V. N. *React. Kinet. Catal. Lett.* **1984**, *26*, 67–72. (d) Housecroft, C. E. *Coord. Chem. Rev.* **1988**, *90*, 111–241.

(22) (a) Baxendale, J. H.; Wells, C. F. *Trans. Faraday Soc.* **1957**, *53*, 800–812. (b) Robertson, A. C. *J. Am. Chem. Soc.* **1926**, *48*, 2072–2082. (c) Davies, G.; Watkins, K. O. *J. Phys. Chem.* **1970**, *74*, 3388–3392.

(23) For example, some of the best methods for electrocatalytic reduction of CO_2 to methanol and other organic chemicals employ pyridine/pyridinium electrocatalysts that require mildly acidic conditions. See: (a) Seshadri, G.; Lin, C.; Bocarsly, A. B. *J. Electroanal. Chem.* **1994**, *372*, 145–150. (b) Cole, E. B.; Lakkaraju, P. S.; Rampulla, D. M.; Morris, A. J.; Abelev, E.; Bocarsly, A. B. *J. Am. Chem. Soc.* **2010**, *132*, 11539–11551.

(24) A recently reported, convenient NMR spectrocopic method enables the accurate determination of solution pH in aqueous fluoride solutions: Gerken, J. B. *J. Fluorine Chem.* **2011**, *132*, 68–70.

(25) The approach to steady state can be slow in some cases. For example, up to 30 min of electrolysis were required to reach steady-state values at low overpotentials. Catalyst redox changes, such as the ones detected by impedance spectroscopy, consume additional current prior to steady-state being reached: Lyons, M. E. G.; Brandon, M. P. *J. Electroanal. Chem.* **2009**, *631*, 62–70.

(26) Inhibition of cobalt-catalyzed water oxidation by phosphate has been reported: (a) refs 21b and 21c. (b) Elizarova, G. L.; Matvienko, L. G.; Lozhkina, N. V.; Maizlish, V. E.; Parmon, V. N. *React. Kinet. Catal. Lett.* **1981**, *16*, 285–288.

(27) The presence of multiple Tafel points at the same overpotential (e.g., the high current-density points in plots 3 and 11) reflects artifacts arising from iR corrections, which were carried out by fitting the raw η/i data to the expression, $d(\eta)/di = b/i + R$ (η = overpotential, i = current, b = Tafel slope, R = resistance). Over- or under-estimation of R by this method can lead to errors in the corrected overpotential. For presentation of this iR correction method, see the following: Kapałka, A.; Fóti, G.; Comninellis, C. *Electrochem. Commun.* **2008**, *10*, 607–610.

(28) Exceptions to this generalization were electrolyses in trifluoromethylsulfonamide buffer ($CF_3SO_2NH_2$, pK_a = 6.3: Koppel, I.; Koppel, J.; Maria, P.-C.; Gal, J.-F.; Notario, R.; Vlasov, V. M.; Taft, R. W. *Int. J. Mass Spectrom. Ion Processes* **1998**, *175*, 61–69. A cobalt-catalyzed degradation pathway may be operative at the anode that leads to the oxidation of the sulfonamide group via intermediates analogous to copper sulfonyl nitrene and cobalt phosphoryl nitrene compounds which have been studied in the context of oxidative amination reactions in organic chemistry:(a) Barman, D. N.; Liu, P.; Houk, K. N.; Nicholas, K. M. *Organometallics* **2010**, *29*, 3404–3412. (b) Lu, H.; Tao, J.; Jones, J. E.; Wojtas, L.; Zhang, X. P. *Org. Lett.* **2010**, *12*, 1248–1251.

(29) Bray, W. C.; Liebhafsky, H. A. *J. Am. Chem. Soc.* **1931**, *53*, 38–44.

(30) For studies of Co-catalyzed disproportionation of H_2O_2, see: ref 22b.

(31) Others have observed polarographic and CV features corresponding to the expected Co(II)/Co(III) and Co(III)/Co(IV) redox couples under alkaline conditions at potentials that support our oxidation-state assignments (a) Benson, P.; Briggs, G. W. D.; Wynne-Jones, W. F. K. *Electrochim. Acta* **1964**, *9*, 281–288. (b) Vittal, R.; Gomathi, H.; Rao, G. P. *J. Electroanal. Chem.* **2001**, *497*, 47–54. (c) Behl, W. K.; Toni, J. E. *J. Electroanal. Chem.* **1971**, *31*, 63–75. (d) Palmas, S.; Ferrara, F.; Vacca, A.; Mascia, M.; Polcaro, A. M. *Electrochim. Acta* **2007**, *53*, 400–406.

(32) Deltombe, E.; Pourbaix, M. In *Atlas D'Équilibres Électrochimiques*; Pourbaix, M., Ed.; Gauthier-Villars: Paris, France, 1963, pp 322−329.

(33) Free energies obtained from refs 9 and 32 were used to construct a Pourbaix diagram in the usual fashion as described in, inter alia, the appendix of ref 34. The goodness of fit between cyclic voltammetry and thermochemical data is, of course, dependent on the quality of the available data. Other free energies for the Co species described here have been reported in the literature (e.g., see ref 34 and references cited therein); however, these gave considerably worse fits to our experimental data at all pH values. See additional content in the Supporting Information and the following reference: Pourbaix, M. In *Atlas D'Équilibres Électrochimiques*; Pourbaix, M., Ed.; Gauthier-Villars: Paris, France, 1963, pp 29−50.

(34) For example, Pourbaix diagrams for cobalt speciation have been constructed that do not include any Co^{IV} compounds at all: Chivot, J.; Mendoza, L.; Mansour, C.; Pauporté, T.; Cassir, M. *Corros. Sci.* **2008**, *50*, 62–69.

(35) The calculated potential in eq 2 is based on application of Nernst's law to the standard free energies obtained from ref 32. In comparison, a linear fit to the data gave $E = 2.11 - 0.171 \cdot pH$ (See Supporting Information).

(36) (a) Venkateswara Rao, K.; Sunandana, C. S. *Solid State Commun.* **2008**, *148*, 32–37. (b) Dutta, P.; Seehra, M. S.; Thota, S.; Kumar, J. *J. Phys.: Condens. Matter* **2008**, *20*, 015218.

(37) Ouyang, B.; Cao, X.; Lin, H. W.; Slane, S.; Kostov, S.; denBoer, M.; Greenbaum, S. G. *Mater. Res. Soc. Symp. Proc.* **1995**, *369*, 59–68.

(38) (a) Dyrek, K.; Sojka, Z. *J. Chem. Soc. Faraday Trans. I* **1982**, *78*, 3177–3185. (b) Holuj, F.; Kwan, C. T. *J. Magn. Reson.* **1975**, *17*, 381–385.

(39) High-spin Co^{II} is typical at octahedral sites in oxide materials, formation of a hexacoordinate S = 1/2 Co^{II} requires a stronger ligand-field: Kataoka, N.; Kon, H. *J. Am. Chem. Soc.* **1968**, *90*, 2978–2979.

(40) Oliva, C.; Forni, L.; Formaro, L. *Appl. Spectrosc.* **1996**, *50*, 1395–1398.

(41) In β-$Co(OH)_2$, no low-temperature EPR spectrum is observed: Al-Ghoul, M.; El-Rassy, H.; Coradin, T.; Mokalled, T. *J. Cryst. Growth* **2010**, *312*, 856–862 (see also ref 38a).

(42) Carretta, P.; Mariani, M.; Azzoni, C. B.; Mozzati, M. C.; Bradarić, I.; Savić, I.; Feher, A.; Šebek, J. *Phys. Rev. B* **2004**, *70*, 024409.

(43) (a) Simmons, G. W.; Kellerman, E.; Leidheiser, H., Jr. *J. Electrochem. Soc.* **1976**, *123*, 1276–1284. (b) Simmons, G. W.; Vértes, A.; Varsányi, M. L.; Leidheiser, H., Jr. *J. Electrochem. Soc.* **1979**, *126*, 187–189. (c) Kulikov, L. A.; Perfil'ev, Y. D.; Kopelev, N. S. *J. Phys. Chem. Solids* **1995**, *56*, 1089–1094.

(44) (a) Risch, M.; Khare, V.; Zaharieva, I.; Gerencser, L.; Chernev, P.; Dau, H. *J. Am. Chem. Soc.* **2009**, *131*, 6936–6937. (b) Risch, M.; Ringleb, F.; Khare, V.; Chernev, P.; Zaharieva, I.; Dau, H. *J. Phys.: Conf. Series* **2009**, *190*, 012167.

(45) Yeo, B. S.; Bell, A. T. *J. Am. Chem. Soc.* **2011**, *133*, 5587–5593.

(46) Dau, H.; Limberg, C.; Reier, T.; Risch, M.; Roggan, S.; Strasser, P. *ChemCatChem* **2010**, *2*, 724–761.

(47) Mockenhaupt, Ch.; Zeiske, Th.; Lutz, H. D. *J. Mol. Struct.* **1998**, *443*, 191–196.

(48) For the specific chemical transformations associated with these layered-oxide redox processes, see Schemes S5, S6, S9, S12, and S14, Supporting Information.

(49) (a) Schwenzer, B.; Neilson, J. R.; Sivula, K.; Woo, C.; Fréchet, J. M. J.; Morse, D. E. *Thin Solid Films* **2009**, *517*, 5722–5727. (b) Bardé, F.; Palacin, M.-R.; Beaudoin, B.; Delahaye-Vidal, A.; Tarascon, J.-M. *Chem. Mater.* **2004**, *16*, 299–306. (c) Delaplane, R. G.; Ibers, J. A.; Ferraro, J. R.; Rush, J. J. *J. Chem. Phys.* **1969**, *50*, 1920–1927.

(50) (a) Costentin, C. *Chem. Rev.* **2008**, *108*, 2145–2179. (b) Huynh, M. H. V.; Meyer, T. J. *Chem. Rev.* **2007**, *107*, 5004–5064. (c) Rosenthal, J.; Nocera, D. G. *Acc. Chem. Res.* **2007**, *40*, 543–553. (d) Mayer, J. M.; Rhile, I. J. *Biochim. Biophys. Acta* **2004**, *1655*, 51–58.

(51) Weibel, A.; Bouchet, R.; Boulc'h, F.; Knauth, P. *Chem. Mater.* **2005**, *17*, 2378–2385.

(52) Other deposition conditions do give rise to layered cobalt oxide materials capable of being analyzed by X-ray diffraction: Benson, P.; Briggs, G. W. D.; Wynne-Jones, W. F. K. *Electrochim. Acta* **1964**, *9*, 275–280. The resulting material remains capable of electrocatalytic water oxidation (ref 31a).

(53) This structural heterogeneity is expressed well by the nomenclature used for similar iron-based deposits: Nishino, Y.; Asakura, Y.; Sawa, T.; Uchida, S.; Ohsumi, K.; Yoshikawa, S.; Amano, O.; Suzuki, N. *J. Nucl. Sci. Technol.* **1991**, *28*, 848–857.

(54) EXAFS data have also been reported for several cobalt-containing layered double-hydroxide materials: Vespa, M.; Dähn, R.; Grolimund, D.; Wieland, E.; Scheidegger, A. *M. Environ. Sci. Technol.* **2007**, *41*, 1902–1908.

(55) (a) Foelske, A.; Strehblow, H.-H. *Surf. Interface Anal.* **2002**, *34*, 125–129. (b) Foelske, A.; Strehblow, H.-H. *Surf. Interface Anal.* **2000**, *29*, 548–555.

(56) XPS sample preparation requirements prevent this technique from revealing the oxidation state of the active catalyst. Indeed, there is doubt as to whether oxidation states above a mixed $Co^{II/III}$ oxide are amenable to XPS. See: Chuang, T. J.; Brundle, C. R.; Rice, D. W. *Surf. Sci.* **1976**, *59*, 413–429.

(57) Matsumoto, Y.; Bando, N.; Hombo, J.; Sasaki, T. *J. Electroanal. Chem.* **1995**, *395*, 45–49.

(58) Butel, M.; Gautier, L.; Delmas, C. *Solid State Ionics* **1999**, *122*, 271–284.

(59) (a) Sakurai, H.; Osada, M.; Takayama-Muromachi, E. *Chem. Mater.* **2007**, *19*, 6073–6076. (b) Ong, N. P.; Cava, R. J. *Science* **2004**, *305*, 52–53 and references therein.

(60) (a) Hertz, J. T.; Huang, Q.; McQueen, T.; Klimczuk, T.; Bos, J. W. G.; Viciu, L.; Cava, R. J. *Phys. Rev. B* **2008**, *77*, 075119. (b) Motohashi, T.; Ono, T.; Katsumata, Y.; Kanno, R.; Karppinen, M.; Yamauchi, H. *J. Appl. Phys.* **2008**, *103*, 07C902. (c) Ren, Z.; Wang, C.; Xu, X.-f.; Cao, G.-h.; Xu, Z.-a.; Zhang, Y.-h. *Chem. Commun.* **2008**, 2155–2157. (d) Motohashi, T.; Ono, T.; Sugimoto, Y.; Masubuchi, Y.; Kikkawa, S.; Kanno, R.; Karppinen, H.; Yamauchi, H. *Phys. Rev. B.* **2009**, *80*, 165114.

(61) (a) Takada, K.; Fukuda, K.; Osada, M.; Nakai, I.; Izumi, F.; Dilanian, R. A.; Kato, K.; Takata, M.; Sakurai, H.; Takayama-Muromachi, E.; Sasaki, T. *J. Mater. Chem.* **2004**, *14*, 1448–1453. (b) Amatucci, G. G.; Tarascon, J. M.; Klein, L. C. *J. Electrochem. Soc.* **1996**, *143*, 1114–1123.

(62) Hem, J. D.; Roberson, C. E.; Lind, C. J. *Geochim. Cosmochim. Acta* **1985**, *49*, 801–810.

(63) Layered Mn oxide materials also exhibit similar water oxidation chemistry: Hocking, R. K.; Brimblecombe, R.; Chang, L.-Y.; Singh, A.; Cheah, M. H.; Glover, C.; Casey, W. H.; Spiccia, L. *Nat. Chem.* **2011**, *3*, 461–466.

(64) Lanson, B.; Drits, V. A.; Silvester, E.; Manceau, A. *Am. Mineral.* **2000**, *85*, 826–838.

(65) Motohashi, T.; Katsumata, Y.; Ono, T.; Kanno, R.; Karppinen, M.; Yamauchi, H. *Chem. Mater.* **2007**, *19*, 5063–5066.

(66) Brossard, L. *J. Appl. Electrochem.* **1991**, *21*, 612–618.

(67) Göhr, H. *Electrochim. Acta* **1966**, *11*, 827–834.

(68) We have previously observed an induction period for CoO_x^{cf} deposition in fluoride buffer (see ref 10). This result can be rationalized by an adsorption/oxidation growth sequence in which the growth is more facile following an initial nucleation event.

(69) Selected references in the context of water oxidation include: (a) Bockris, J. O'M. *J. Chem. Phys.* **1956**, *24*, 817–827. (b) Gnanamuthu, D. S.; Petrocelli, J. V. *J. Electrochem. Soc.* **1967**, *114*, 1036–1041. (c) Hamann, C. H.; Hamnett, A.; Vielstich, W. *Electrochemistry*; Wiley-VCH: Weinheim, Germany, 2007.

(70) Elizarova, G. L.; Zhidomirov, G. M.; Parmon, V. N. *Catal. Today* **2000**, *58*, 71–88.